Lava Discharge Rate of Sinabung Volcano Obtained from Modis Hot Spot Data

Estu Kriswati and Akhmad Solikhin

Centre for Volcanology and Geological Hazard Mitigation,
Geological Agency, Ministry of Energy and Mineral Resources
Jalan Diponegoro 57, Bandung

Corresponding author: estukriswati@gmail.com
Manuscript received: October, 07, 2019; revised: December, 19, 2019;
approved: February, 20, 2020; available online: September, 17, 2020

Abstract - To find out the long term data of Sinabung magma discharge rate and how long a series of eruption will be ended, time series of the volume of magma discharge is required. The dominant eruption product is pyroclastic flow that begins with the growth of the lava dome, so it is important to determine the volume of the lava dome over time. The method of determining the volume of magma issued is carried out by using hotspot data to resolve the problem of prevented visual observations and ground measurements. The heat and volume flux data expressed within a long period for a better view of variations in the Sinabung volcanic activity are based on thermal satellite data. Related lava dome volume and seismic data are also displayed to be compared with the heat and volume flux data. The numbers of thermally anomalous pixels and sum of radiance for all detected pixels at Sinabung during an overpass in the period of 2014 to 2018 have a downward trend. The discharge rates in the period of January 2014 to April 2015, Mei 2015 to March 2016, April 2016 to March 2017, and June 2017 to February 2018 are 0.86 m³/sec, 0.59 m³/sec, 0.36 m³/sec, and 0.25 m³/sec, respectively. Assuming no new intrusion or deformation rate changes, the lava discharge will be in the lowest rate in the early 2020s.

Keywords: discharge rate, MODIS hotspot, Sinabung Volcano, volume of lava dome

Introduction

Remote sensing approach by using instruments, operating at different wavelengths from the ultraviolet to microwave regions of the electromagnetic spectrum, has long been recognized as a worthwhile tool to monitor volcanoes, to study volcanic processes, and to map volcanic products throughout an eruption cycle from pre-eruption repose to post-eruption relaxation. Remote sensing also plays an important role when ground-based volcano monitoring and fieldwork are dangerous or impossible due to natural (eruptive activity, difficult terrain, dense vegetation, *etc*.) or political conditions (Head *et al*., 2012). There have been many studies on Indonesian volcanoes by applying remote sensing techniques; using high spatial resolution optical images (*e.g.* Solikhin *et al*., 2012; 2015b), radar images (Agustan *et al*., 2010; Saepuloh *et al*., 2012; Solikhin *et al.,* 2015a), as well as thermal infrared images (Harris and Ripepe, 2007; Carr *et al*., 2016).

Infrared observations have particular utility in the study of active volcanoes by virtue the very

nature of volcanism which is associated with the transfer of heat to the surface (Oppenheimer, 1998). The thermal emittance of a volcanic surface relates to its activity at a specific time, which may consist of active lava flow, lava lake, or lava dome, a system of fumaroles or a more subtly radiant surface heated by shallow magma intrusions. As a result, infrared observations may indicate impending changes in activity, or may simply provide information as to a particular volcano activity status. Infrared remote sensing has relatively been common since the early 1960s, and then developed with subsequent sensors that were launched along with improvements in spectral and spatial resolution (Blackett, 2017). Various satellite instruments, which have infrared observational functionality and are able to provide global and regional volcanic hotspots on an hourly to daily basis, have been widely used for monitoring the eruptive state of active volcanoes (*e.g.* Harris *et al*, 2000; Wright *et al*., 2004; Jay *et al*., 2013, Blackett, 2017). Many automated algorithms have also been developed and applied to infrared satellite data in order to detect volcanic thermal anomalies, one of which is MODVOLC, the MODIS (Moderate Resolution Imaging Spectroradiometer) volcanic hot spot detection algorithm (Wright *et al*., 2002). This study illustrates the use of MODVOLC thermal radiance data in approaching temporal variations of the Sinabung eruptive activity.

Sinabung Volcano in Karo District, North Sumatra Province (Figure 1) entered into a renewed phase of activity on September 2013. Starting on 30 December 2013, Sinabung Volcano showed a high level of activity characterized by incandescent ejected materials and lava dome growth followed by dome collapse resulting in pyroclastic flows and lava avalanches. During this period, the product of Sinabung was dominated by fresh pyroclastic flow deposits generated from lava dome collapses. Therefore, estimating the volume of lava dome from time to time is very important for this volcano hazard analysis. However, fog sometimes prevented visual observations of Sinabung, thus ground
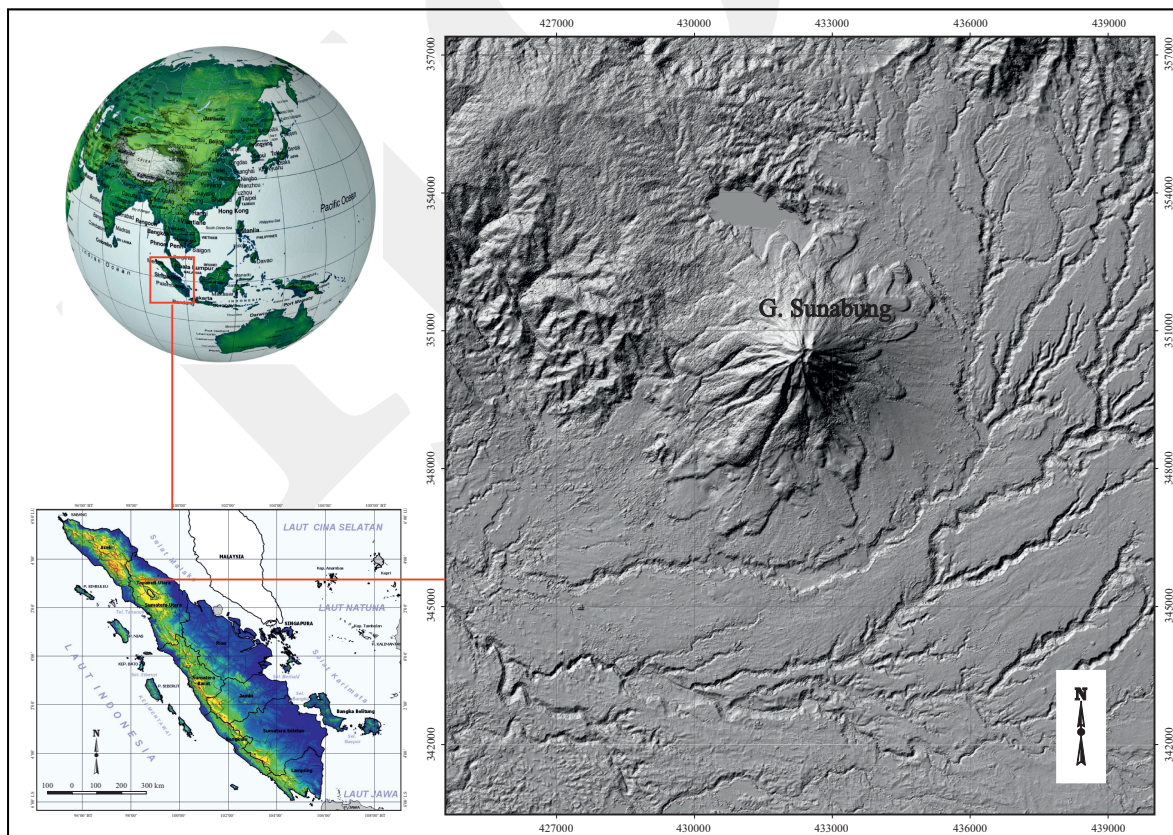
Figure 1. Location map and digital elevation model of Sinabung Volcano (source: Remote Sensing Application Centre, LAPAN, 2007).

measurement of lava domes cannot be performed frequently. Therefore, implementation of remote sensing technique to determine the volume of lava dome can be a very appropriate option.

In this study, thermal radiance data were converted into heat and volume flux data to estimate the volume of magma discharge. The results are examined based on thermal satellite data by comparing them with seismic data and ground measurement. The objectives of this study are to estimate magma discharge rate of Sinabung and to observe its variations over a long period (2014−2018) for a better view of volcanic activity variations as well as to predict the length of the eruption period.

The 2013-2017 Sinabung Eruptions

Sinabung Volcano had been dormant when it began erupting again in August 2010 and entered into a renewed phase of activity on September 2013 with intense volcanic eruption. The series of eruption has been occurred since 15 September 2013 and been producing pyroclastic flows, when the continuously extruded magma accumulates in the crater forming a lava dome and regularly collapses. At the time of this writing (mid-September 2019), Sinabung activity was remaining in an eruption stage with a relatively lower intensity characterized by several gas burst events. Figure 2 shows the number of eruption, avalanche, and py-
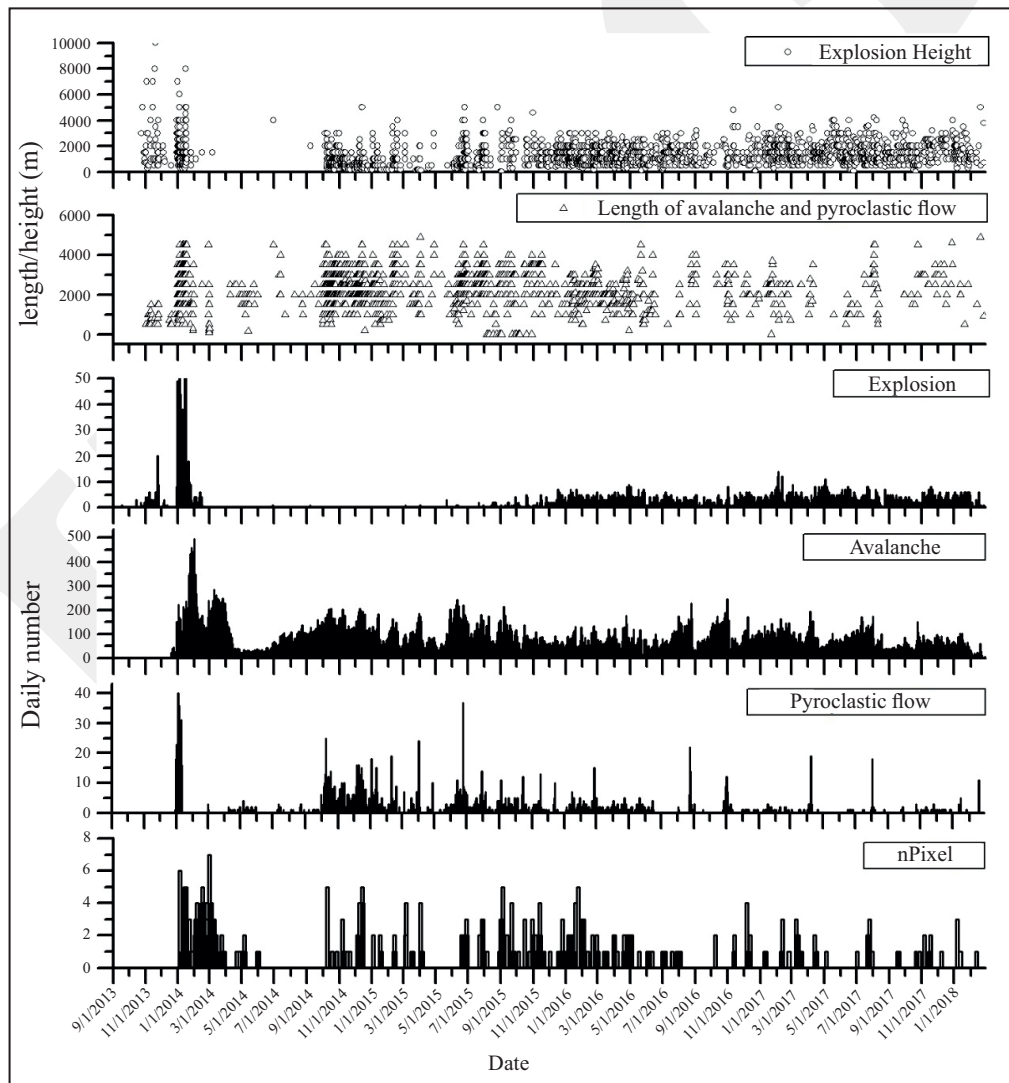
Figure 2. The activities of Sinabung Volcano for the period September 2013 to February 2018, represented by charts of (from top to bottom) ash column height (explosion height), length of avalanche and pyroclastic flow, number of eruptions (explosions), number of rock avalanche events, number of pyroclastic flow events, as well as number of MODIS hotspot pixel.

roclastic flow events, together with its heights for ash column as well as its travel distance for lava avalanche and pyroclastic flows, which reflects the activity of Sinabung in the period of September 2013 to February 2018. The explosion reached a height of up to 10 km on 19 November 2013. Incandescent ejected materials reached an area in the distance up to 800 m, and the pyroclastic flows reached 4 km from the summit to the southeastern slope and 3.5 km to the southern slope of Sinabung on January 2014.

On January 2014, ash plumes rose as high as 5 km, pyroclastic flows travelled 0.5 - 4.5 km to the east, southeast, and south, and incandescent material was observed as far as 3 km to the southeast and east. During February to April 2014, the column eruption height decreased, and has a month break during May 2014. The activity was characterized by dome growth and was accompanied by a lava flow that was frequently visibly incandescent since February 2014. The eruption started again at the end of June 2014, the eruption plume rose to 2 km above the crater, and pyroclastic flows extended 4.5 km to the south and southeast. The lava lobe grew to the southeastern slope with the length increased from 2 km on February to 3 km on December 2014.

During the period of January until the end of June 2015, the column eruption reached a height up to 5 km above the summit, and the lava lobe growth up to 3 km to the southeastern slope, lava avalanche as well as block and ash pyroclastic flow reached the distance up to 4.5 km to the south and southeast. On June, the lava dome volume had increased to more than 3 million m³ (Mm³) and was unstable. On January 2016, the column of ash reached a height up to 6.1 km above the summit drifting 15 - 55 km away from the volcano, and the lava lobe growth up to 2.95 km to the southeastern slope, glowing avalanche reached 1 km away to southern-southeastern, block and ash pyroclastic flow reaching the distance up to 4.5 km to the south and southeastern. On May 21 2016, the pyroclastic flow reached 4.5 km distance and the surge hit Gamber Village, burned houses, and killed nine people.

The eruption continued in 2017 with decreasing intensity, the ash cloud reached a height up to 5 km above the summit, lava avalanche 1 km to the southern-southeastern, block and ash pyroclastic flow reached the distance up to 2 km to the south and southeast.

METHOD AND DATA

Method

Hotspot observation can be done using several satellite sensors such as AVHRR, MODIS, and GOES. To obtain radiance data for the Sinabung Volcano output from the MODIS volcanic hot spot, detection algorithm (MODVOLC) was used. MODVOLC is a non-interactive algorithm developed at the Hawaii Institute of Geophysics and Planetology (HIGP) that uses low spatial resolution (1 km pixel-size) infrared satellite data acquired by the MODIS to detect and to map the global distribution of volcanic thermal anomalies in near-real-time (Wright *et al.*, 2002). MODVOLC scans the Level-1B MODIS data stream, on a pixel-by-pixel basis, for evidence of pixel and subpixel-sized high-temperature radiators.

The MODIS detects the presence of high temperature (hotspot) on the surface of the volcano which is presented in the form of pixels by comparing the results of calculations between infrared short waves and infrared long waves. The calculations of these infrared waves are formulated by Wright *et al.,* (2004; 2008) as Normalized Temperature Index as follow:

$$NTI = \frac{Band\ 22 - Band\ 32}{Band\ 22 + Band\ 32} \qquad \begin{array}{l} Band\ 22: 4\ microns \\ Band\ 32: 12\ microns \end{array}$$

If Band 22 is saturated, then Band 21 is used to replace Band 22. When the value of NTI is greater than -0.8, then the pixel is marked as a warning that a hotspot has been detected in the area. The hot spot details (location, emitted spectral radiance, time, satellite observation geometry) are written to ASCII text files and transferred via FTP

to HIGP, from where the results are disseminated via the internet. These data can be used to determine the presence, radiant intensity, and heat flux of volcano-related hot spots (*e.g.* Wright *et al.,* 2004).

The MODVOLC radiance data are used to estimate heat and volume fluxes on Sinabung Volcano by applying the methodology developed by Harris *et al.* (1997a, 1997b, 1998, 2003). The lava area is calculated by assuming that a pixel hot spot contains a hot (lava) source at temperature T_h surrounded by a cooler (ambient) background at T_b. Together these two sources contribute to the pixel integrated temperature (T_{int}), thus:

$$L(T_{int},\lambda) = p\,L(T_h, \lambda) + (1 - p)\,L(T_b, \lambda)$$

in which L is the Planck function for a blackbody radiating at temperature T and wavelength λ, and p is the pixel portion occupied by the hot source (Oppenheimer *et al.*, 1993). Following Wright and Flynn (2004), T_{int} from MODIS band 21 (3.939 mm) pixel-integrated radiances are obtained, given in the MODVOLC text files. This waveband is highly sensitive to subpixel hot spots. The background temperature is obtained from band 32 (12.02 mm) pixel-integrated radiances. This waveband is less sensitive to subpixel hot spots. The signal is then assumed to be dominated by the ambient background (Wright and Flynn, 2004).

Thermal radiance data for each detected hot spot were converted to heat flux (in units of joules per second) and volume flux (in m³ per second), based on the method and computing technique of Harris and Ripepe (2007). Calculation of the volume flux (E) from estimated heat fluxes follows the equation below:

$$E = Q_{tot} / \rho\,(c_p\,\Delta T + L\,\mu)$$

The total heat loss Q_{tot} can be estimated from the sum of heat flux radiative [$Q_{rad} = A\sigma\varepsilon T_h^4$] and heat flux convective [$Q_{conv} = h_c\,(T_h - T_{air})$] where:

σ, ε, hc, and T_{air} are the Stefan-Boltzmann constant.

$\sigma = 5.67 \times 10^8$ W m^{-2} K^{-4},

ε is emissivity of Andesite (0.98 [Salisbury and D'Aria, 1992, 1994]);

h_c is convective heat transfer coefficient for active lava (~50 W m^{-2} K^{-1}),

T_h is surface temperature,

T_{air} is ambient air temperature (25C).

ΔT is post extrusion cooling of the unit interior (200 - 350°C; Harris *et al.*, 2003),

L is latent heat of crystallization (3.5 x 10^5 J/ kg K), and

μ is post eruption crystallization (0.45 for Sinabung).

The calculation of Q_{tot} assumes surface heat losses dominate the thermal budget, and that heat loss by basal conduction from a dome overlying an active conduit is not significant. Sinabung lava density (ρ = 2500 kg/m³; Nakada, 2018) and specific heat capacity (cp = 1150 J/kg K) are corrected for vesicularity of 10 - 30 %. The lava temperature range gives two end member heat flux cases, a cold heat flux (T_h = 150°C, ΔT = 200°C, vesicularity 10%), and hot (T_h = 270°C, ΔT = 350°C, vesicularity 30%).

Data

MODIS sensors are flown on NASA's Terra and Aqua satellites. These two polar orbiting satellites have the return periods of twelve hours, so that any point on the earth surface can be imaged twice a day by each satellite (if cloud-free), for a total of four images per day using both satellites. Overpass times for Terra are 15:00 and 03:00, and for Aqua 06:00 and 18:00 (all times are UTC). During January 2014 to February 2018, hot spots were detected by MODVOLC at Sinabung given a total of 429 overpasses by Terra and Aqua. Less hot spots were detected by MODVOLC due to low intensity activities and/or cloud cover and/ or ash cloud from eruption or pyroclastic flows that prevented hot spot detection. The consistent long-term trends, confirmed by similar radiances recorded across multiple data points that can reveal changes in eruptive activity (*e.g.* Harris *et al.*, 1997a; Wright *et al.*, 2002).

RESULTS

Sinabung 2014 - 2017 Hotspot Data

At Sinabung, the number of thermally anomalous pixels detected during an overpass in the period of 2014 to 2018 has a downward trend (Figure 3a). The maximum band 21 radiance (B21max) for detected pixels, also decreased from a mean ($\pm 1s$) of 1.4 ± 1.1 Wm^{-2} sr^{-1} μm^{-1} (Figure 3b), with anomaly on 2 September 2015 and 10 January 2016. The Band 21 radiance summed for all detected pixels during an overpass (SB21) showed an identical trend, with the mean decreasing from 3.2 ± 2.9 in the period of 2014 to 1.5 ± 1.0 Wm^{-2} sr^{-1} μm^{-1} in the period of 2017−2018 (Figure 3c).

Heat and Volume Flux

During the period of 2014 - 2018, heat fluxes from detected hotspots for Sinabung were obtained in the range of 0.5 to 51.9 x 10^8 J/sec (Figure 4). These convert to volume fluxes in the range of 0.04 to 4.8 m^3/sec, with a mean of 0.7 m^3/sec. The total power and volume for periods of high volcanic activity can be obtained by integrating heat flux and volume through time intervals. The total power for the period of 2014 - 2018 is 7.5 x 10^{16} J and converted to the total volume of 6.9 x 10^7 m^3 (Figure 5).
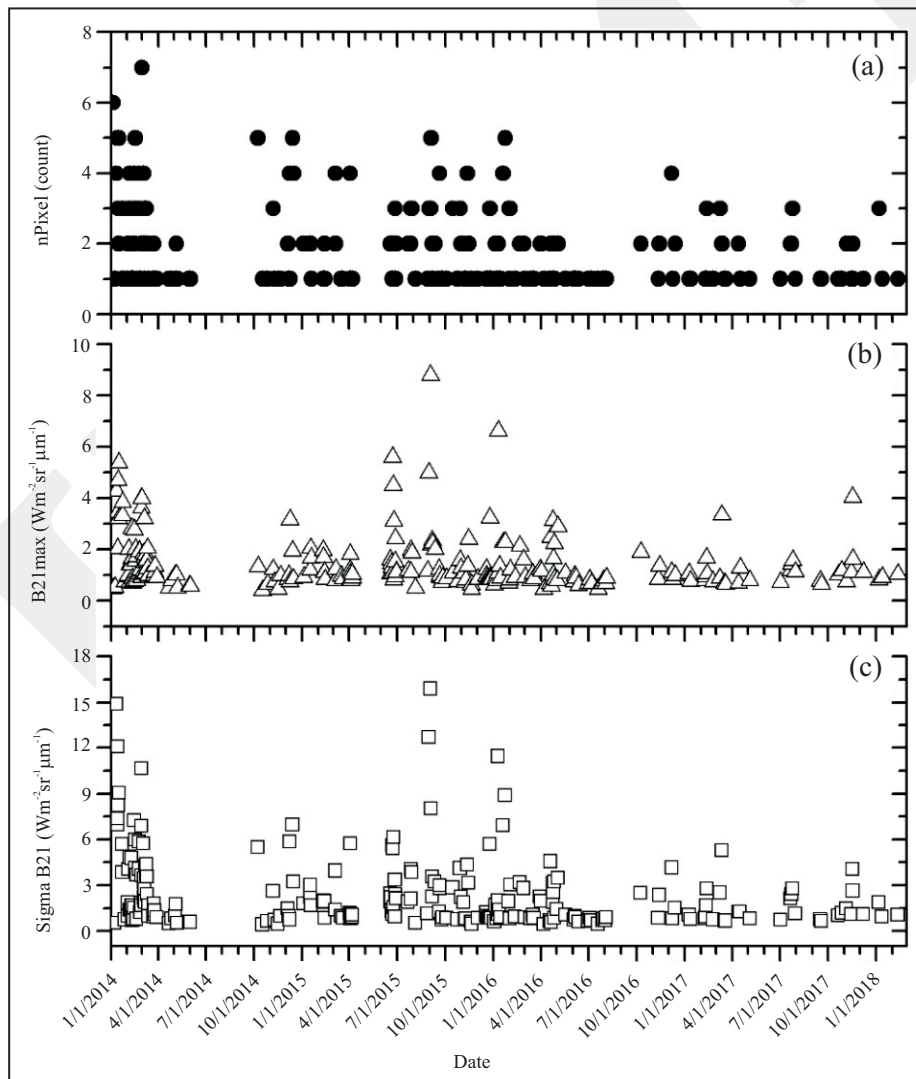
Figure 3. (a) The number of thermally anomalous pixels detected by MODVOLC, (b) maximum Band 21 radiance (B21max) for detected pixels, and (c) the sum of all Band 21 pixel radiances (SB21) detected during each overpass for Sinabung in the period of January 1, 2014, to February 11, 2018.
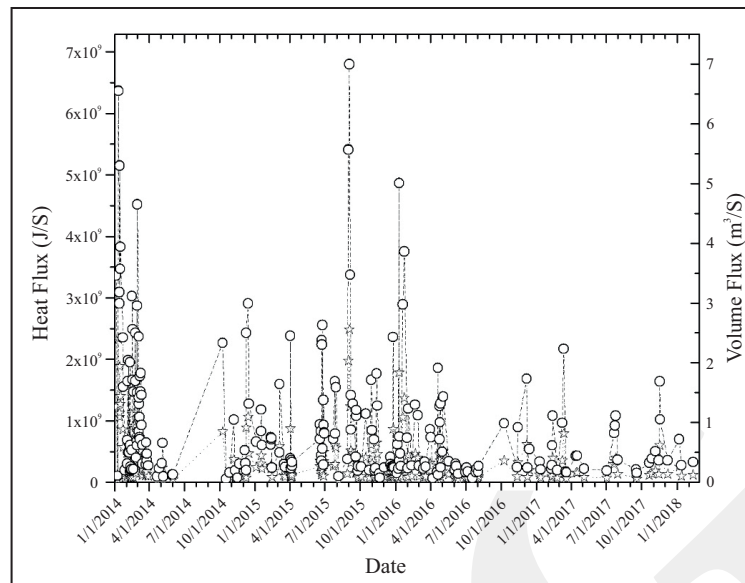
Figure 4. Heat and volume flux ranges calculated using MODVOLC data for Sinabung during January 2014 to February 2018. The maximum heats or volume fluxes denoted by circles and the minimum denoted by stars.
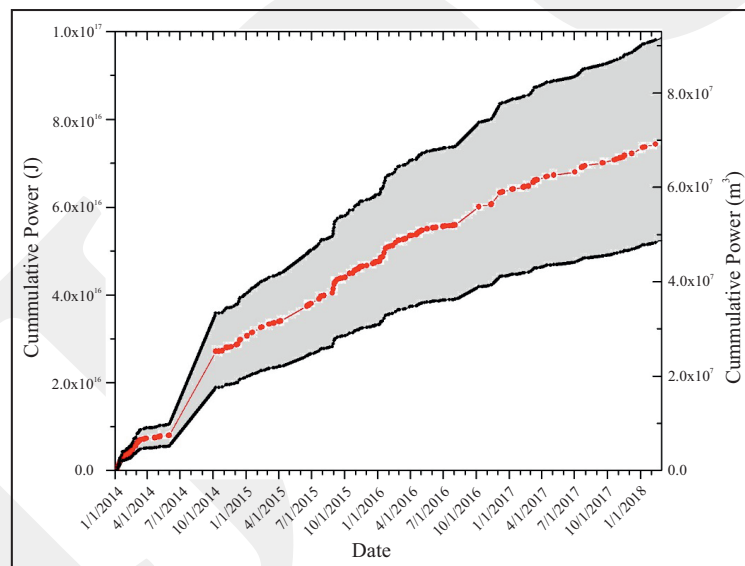
Figure 5. Envelope of cumulative power and volume (gray zone) for Sinabung from integration heat and volume fluxes given in Figure 4.

DISCUSSION

Measured Volume of Lava Flow and Dome

The lava grew to the southeastern slope with the length of 2,200 - 2,500 m during February - March 2015. It increased to approximately 2,641 m in April, and extended to ± 2,833 m in May, ± 2850 m on June, and ± 2,885 - 2,905 m throughout July−August, ± 2,935 m on September, and ± 2,946 m on October−December 2015 (Figure 2).

Sinabung lava dome volume measurements were performed using a laser distance meter started on May 23, 2015. The horizontal and vertical distances were measured between the targets and the reference points (beside the growing lava dome) from the Centre for Volcanology and Geological Hazard Mitigation (CVGHM) Sinabung Volcano Observatory (approximately 8 km away from the volcano). The calculation of the volume was done by assuming a rectangular block shape (Figure 6).

247

Figure 6. Measurement of lava dome volume.

On May 21, 2016, the volume of material released in multiple avalanches was estimated 2 Mm³. After the events, lava dome began to grow with the growth rate showed an increase from May 22 to June 6, 2016, and reached a total volume of 2.6 Mm³ before a series of hot and erupting clouds on August 24, 2016. After an increase in activity on the August 24−26 that brought down all lava domes of 2.6 Mm³, the lava dome again grew at a slow rate (Figure 7), and again showed an increase in speed at the beginning of October 2016. On September 26, the volume of the lava dome was measured at 0.9 Mm³, on October 2 it measured 1.4 Mm³, and on October 4 it measured 1.6 Mm3. The growth of the lava dome again peaked at the end of October 2016 with a measured volume

of approximately 2.5 Mm³. On the first week of November, the lava dome was completely fed in several hot clouds. Throughout the month of December 2016, the growth of lava domes can be said to be very slow and even experienced a slowdown in mid-December. Significant growth took place on early January 2017 even though it slowed again at the end of January, even until the end of March 2017. On March 15 and 20, 2017, the measurements were 1.7 Mm³ and 1.3 Mm³ respectively. In the period from March to June 2017, the growth of lava domes showed a significant increase in volume. At the beginning of July 2017 a volume of approximately 2.6 Mm³ was measured. The total volume of lava dome during the period of May 2015 to February 2018 was 6.7 x 10⁷ m³.

Previous Volume Estimation

Some researchers have calculated the volume of material discharge during the eruption of Sinabung Volcano since 2013. Nakada *et al.* (2018) calculated the lava discharge rate during 2013–2015 eruption. The volume was calculated by combining topographic measurement and remote sensing imagery data as well as thermal camera. The highest level of lava discharge rate occured at the initial stage and then decreased
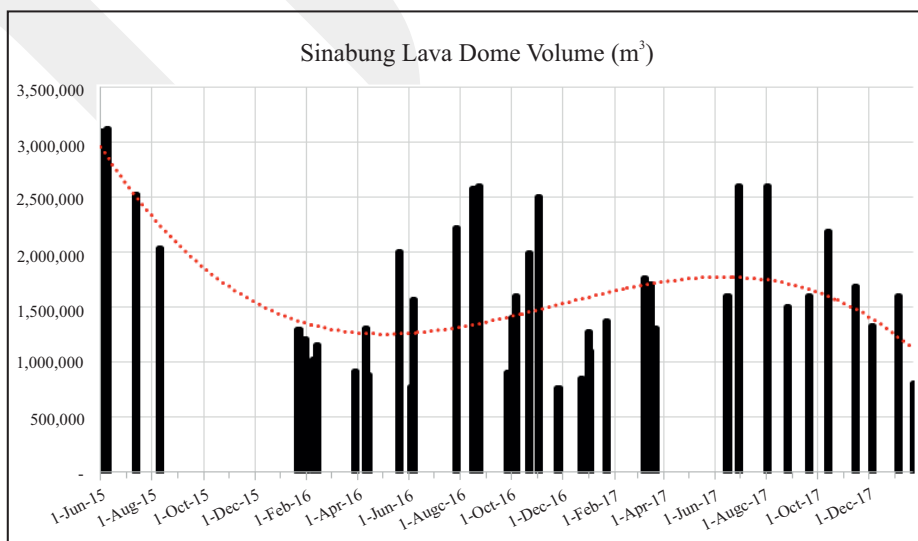
Figure 7. The measured volume of Sinabung lava dome May 2015 to February 2018 (bar graph). Assuming the change in volume as polynomial trend, there will be three periods of different rate (dot line).

exponentially over time. The rate of addition of new lava material was estimated on April 2015 to be around ~ 0.7 m³/s and to < 0.5 m³/s since the summer of 2015. The discharge rate is close to the results of GPS measurements by Hotta *et.al*. (2017). The linear trend of cumulative volume change of the deformation source from the 2014 period until May 2016 showed the decline rate. Yulianto *et al*. (2016) estimated the volume of lava and pyroclastic deposits using digital elevation models (DEMs) for the period of 2010–2015. The results showed that the estimated total volume of lava and pyroclastic deposits, produced during the period of 2010 to mid-2015, was approximately 2.8×10^8 m³. According to Nakada *et al*. (2018), the result was overestimate because of the differ-ent in deposit thickness measurement approach.

Based on the previous estimation of discharge rate and the measurement of lava dome (Figure 7), the eruption period was divided into four phases: (1) January 2014 to April 2015, (2) Mei 2015 to March 2016, (3) April 2016 to March 2017, and (4) June 2017 to February 2018. Table 1 shows the volume discharge rate resulting from Sinabung activity over time.

In the period (1) and (2), the rate between three calculations is similar. In the period of (3) and (4) the different between lava dome measurement and hotspot calculation has significant different. The differences appear related to hot spots which were less detected by MODVOLC due to ash cloud from the eruption that prevented hot spot detection. This is supported by the number of explosions and height of the ash column occuring in Sinabung after April 2016 (Figure 2).

Predicting the Length of Eruption Period

By using the cumulative volume change of the deformation source data compared with the best fit exponential function, Hotta *et al*. (2017) (Figure 8a) concluded that magma effusion would terminate in the early 2020s, assuming no new intrusion or deformation rate changes. This research has resulted in a significantly lower rate of lava discharge from 2014 to 2018. By taking the middle of each period plotted as x-axis and discharge rate as y-axis, it forms an exponential graph as shown in Figure 8b. The lava discharge will be in the lowest rate in the early 2020s, giving the same result with a previous research.

Table 1. Comparison of Discharge Rate from Measurement Data and the Previous Research

	(1)	**(2)**	**(3)**	**(4)**
Lava dome measurement	-	0.6 m³/s	0.9 m³/s	0.6 m³/s
Nakada *et al*. (2018)	~ 0.7 m³/s	< 0.5 m³/s	-	-
This study	0.86 m³/s	0.59 m³/s	1.36 m³/s	1.25 m³/s
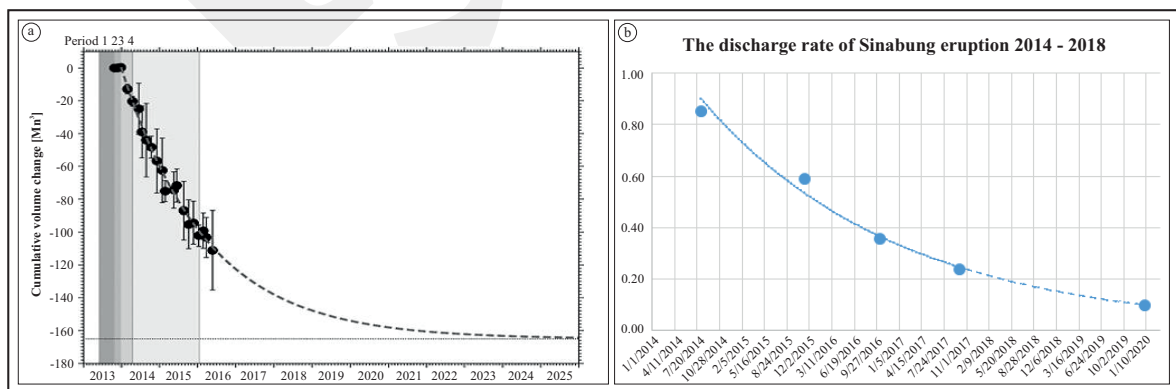
Figure 8. (a) Comparison of the cumulative volume change of the deformation source (black dots) with the best fit exponen-tial function (the gray dashed line; Hotta *et al*., 2017). (b) Plotting the discharge rate from 2014 to 2018 (dot) and predicted lowest rate with assumption no new intrusion by the best fit exponential function (line and dot line).

Conclusion

The Sinabung volcanic activity can be detected based on thermal satellite data. The numbers of thermally anomalous pixels and the sum of radiance for all detected pixels at Sinabung during an overpass in the period 2014 to 2018 have a downward trend. The total volume of January 2014 to February 2018 is 6.9×10^7 m³. The discharge rate in the period of January 2014 to April 2015, Mei 2015 to March 2016, April 2016 to March 2017, and June 2017 to February 2018 were 0.86 m³/sec, 0.59 m³/sec, 0.36 m³/sec, and 0.25 m³/sec, respectively. Assuming no new intrusion or deformation rate changes, the lava discharge will be in the lowest rate in the early 2020s.

Furthermore, the total volume of lava dome from ground measurement during the period of May 2015 to February 2018 gave the result of 6.7×10^7 m³. The discharge rates in the period of Mei 2015 to March 2016, April 2016 to March 2017, and June 2017 to February 2018 were 0.6 m³/sec, 0.9 m³/sec, and 0.6 m³/sec, respectively.

The differences of the rate appear related to obstruction of hot spots by ash column. Seismic data show the increase in number of explosions that prevented hot spot detection. The results of the calculations of lava volume from these two methods give the impression that the volume calculation based on detected hotspot is not suitable to the volcano with high activity of ash explosion. But to look at trends in volume changes and to forecast when the eruption will stop, the calculation of volume from hotspot data can be used.

Acknowledgment

References

Agustan, Kimata, F., Abidin, H.Z., and Pamitro, Y.E., 2010. Measuring ground deformation of the tropical volcano, Ibu, using ALOS-PALSAR data. *Remote Sensing Letters*, 1, 37-44. DOI:10.1080/01431160903246717

Blackett, M., 2017. An Overview of Infrared Remote Sensing of Volcanic Activity. *Journal of Imaging,* 3, 13.

Carr, B.B., Clarke, A.B., and Vanderkluysen, L., 2016. The 2006 lava dome eruption of Merapi Volcano (Indonesia): Detailed analysis using MODIS TIR. *Journal of Volcanology and Geothermal Research,* 311, p.60-71. DOI:10.1016/j.jvolgeores.2015.12.004

Harris, A.J.L. and Stevenson, D.S., 1997a. Magma budgets and steady state activity of Vulcano and Stromboli. *Geophysical Research Letters,* 24, p.1043-1046. DOI:10.1029/97gl00861

Harris, A.J.L. and Stevenson, D.S., 1997b. Thermal observations of degassing open conduits and fumaroles at Stromboli and Vulcano using remotely sensed data. *Journal of Volcanology and Geothermal Research,* 76 (3-4), p.175-198. DOI:10.1016/s0377-0273(96)00097-2

Harris, A.J.L., Flynn, L.P., Keszthelyi, L., Mouginis-Mark, P.J., Rowland, S.K., and Resing, J.A., 1998. Calculation of lava effusion rates from Landsat TM data. *Bulletin of Volcanology,* 60, p.52-71. DOI:10.1007/s004450050216

Harris, A.J.L., Flynn, L.P., Dean, K., Pilger, E., Wooster, M., Okubu, C., Mouginis-Mark, P., Gerbeil, H., Thornber, C., De la Cruz-Reyna, S., Rothery, D., and Wright, R., 2000. Real-time satellite monitoring of volcanic hot spots. *In*: Mouginis-Mark, P., Crisp, J.A., and Fink, J.H. (eds.), *Remote sensing of active volcanism: American Geophysical Union Research,* 76, p.175-198. DOI:10.1029/gm116p0139

Harris, A.J.L., Rose, W.I., and Flynn, L.P., 2003. Temporal trends in lava dome extrusion at Santiaguito 1922-2000. *Bulletin Volcanology,* 65, p.77-89, DOI 10.1007/s00445-002-0243-0.

Harris, A.J.L. and Ripepe, M., 2007. Regional earthquake as a trigger for enhanced volcanic activity: Evidence from MODIS thermal data, *Geophysical Research Letters,* 34, L02304, DOI:10.1029/2006GL028251, 2007.

Head, E.M., Maclean, A.L., and Carn, S.A., 2012. Mapping lava flows from Nyamuragira Volcano (1967–2011) with satellite data and automated classification methods. Geomatics, *Natural Hazards and Risk,* 4, p.119-144. DOI:10.1080/19475705.2012.680503

Hotta, K., Iguchi, M., Ohkura, T., Hendrasto, M., Gunawan, H., Rosadi, U., and Kriswati, E., 2017. Magma intrusion and effusion at Sinabung Volcano, Indonesia, from 2013 to 2016, as revealed by continuous GPS observation, *Journal of Volcanology and Geothermal Research*, 382, p.173-183. DOI: 10.1016/j.jvolgeores.2017.12.015.

Jay, J.A., Welch, M., Pritchard, M.E., Mares, P.J., Mnich, M.E., Melkonian, A.K., Aguilera, F., Naranjo, J.A., Sunagua, M., and Clavero, J., 2013. Volcanic hotspots of the central and southern Andes as seen from space by ASTER and MODVOLC between the years 2000 and 2010. *Geological Society, London, Special Publications,* 380, p.161-185. DOI:10.1144/sp380.1

LAPAN, 2007. Informasi Spatial Penginderaan Jauh Digital Elevation Model - SRTM Pulau Sumatera, Pusat Pengembangan Pemanfaatan dan Teknologi Penginderaan Jauh, Lembaga Penerbangan dan Antariksa Nasional (LAPAN), http://www.rs.lapan.go.id.SIMBA

Nakada, S., Zaennudin, A., Yoshimoto, M., Maeno, F., Suzuki, Y., Hokanishi, N., Sasaki, H., Iguchi, M., Ohkura, T., Gunawan, H., and Triastuty, H., 2018. Growth process of the lava dome/flow complex at Sinabung Volcano during 2013–2016, *Journal of Volcanology and Geothermal Research*, 14 (1), p.40-50. DOI: 10.1016/j.jvolgeores.2017.06.012.

Oppenheimer, C., 1993. Thermal distributions of hot volcanic surfaces constrained using three infrared bands of remote sensing data. *Geophysical Research Letters,* 20, p.431-434. DOI:10.1029/93gl00500

Oppenheimer, M., 1998. Global warming and the stability of the West Antarctic Ice Sheet. *Nature,* 393, p.325-332. DOI:10.1038/30661

Saepuloh, A., Koike, K., and Omura, M., 2012. Applying Bayesian Decision Classification to Pi-SAR Polarimetric Data for Detailed Extraction of the Geomorphologic and Structural Features of an Active Volcano. *IEEE Geoscience and Remote Sensing Letters,* 9, p.554.558. DOI:10.1109/lgrs.2011.2174611

Salisbury, J.W. and D'Aria, D.M., 1992. Emissivity of terrestrial materials in the 8–14 μm atmospheric window. *Remote Sensing of Environment,* 42, p.83-106. DOI:10.1016/0034-4257(92)90092-x

Salisbury, J.W. and D'Aria, D.M., 1994. Emissivity of terrestrial materials in the 3–5 μm atmospheric window. *Remote Sensing of Environment,* 47, p.345-361. DOI:10.1016/0034-4257(94)90102-3

Solikhin, A., Thouret, J.C., Gupta, A., Harris, A.J.L., and Liew, S.C., 2012. Geology, tectonics, and the 2002–2003 eruption of the Semeru Volcano, Indonesia: Interpreted from high-spatial resolution satellite imagery. *Geomorphology,* 138, p.364-379. DOI:10.1016/j.geomorph.2011.10.001

Solikhin, A., Pinel, V., Vandemeulebrouck, J., Thouret, J.C., and Hendrasto, M., 2015a. Mapping the 2010 Merapi pyroclastic deposits using dual-polarization Synthetic Aperture Radar (SAR) data. *Remote Sensing of Environment,* 158, p.180-192. DOI:10.1016/j.rse.2014.11.002

Solikhin, A., Thouret, J.C., Liew, S.C., Gupta, A., Sayudi, D.S., Oehler, J.F., and Kassouk, Z., 2015b. High-spatial-resolution imagery helps map deposits of the large (VEI 4) 2010 Merapi Volcano eruption and their impact. *Bulletin of Volcanology,* 77 (3), p1-23. DOI:10.1007/s00445-015-0908-0

Wright, R., Flynn, L.P., Garbeil, H., Harris, A.J.L., and Pilger, E., 2002. Automated volcanic eruption detection using MODIS, *Remote Sensing of Environment* 82, p.135-155. DOI:10.1016/s0034-4257(02)00030-5

Wright, R., Flynn, L.P., Garbeil, H., Harris, A.J.L., and Pilger, E., 2004. MODVOLC: near-real-time thermal monitoring of global volcanism. *Journal of Volcanology and Geothermal Research*, 135, p.29-49. DOI:10.1016/j.jvolgeores.2003.12.008

Wright, R. and Pilger, E., 2008. Radiant flux from Earth's subaerially erupting volcanoes, *International Journal of Remote Sensing,* 29, (22), p.6443-6466. DOI:10.1080/01431160802168210

Yulianto, F., Suwarsono, and Sofan, P., 2016. The Utilization of Remotely Sensed Data to Analyze the Estimated Volume of Pyroclastic Deposits and Morphological Changes Caused by the 2010–2015 Eruption of Sinabung Volcano, North Sumatra, Indonesia. *Pure and Applied Geophysics*, 178 (8), p.2711-2725. DOI: 10.1007/s00024-016-1342-8.